



On dislocation interaction with radiation-induced defect clusters and plastic flow localization in fcc metals

N. M. GHONIEM†, S.-H. TONG

Mechanical and Aerospace Engineering Department, University of California,
Los Angeles, California 90095-1597, USA

B. N. SINGH

Materials Research Department, Risø National Laboratory,
DK-4000 Roskilde, Denmark

and L. Z. SUN

Civil and Environmental Engineering Department, The University of Iowa,
Iowa City, Iowa 52242, USA

[Received 7 December 1999 and accepted in revised form 26 February 2001]

ABSTRACT

Plastic instability associated with formation of narrow flow channels results from dislocation pinning–unpinning by defect clusters. We investigate the dynamics of dislocation interaction with radiation-induced defect clusters, and specifically with, firstly, sessile self-interstitial atom clusters in dislocation decorations and, secondly, stacking-fault tetrahedra (SFTs) in the matrix. It is shown that the critical stress to free trapped dislocations from pinning atmospheres can be a factor of two smaller than values obtained on the basis of rigid dislocation interactions. The unpinning mechanism is a consequence of the growth of morphological instabilities on the dislocation line. Dislocation sources are activated in spatial regions of low SFT density, where their destruction by glide dislocations leads to subsequent growth of localized plasticity in dislocation channels. We show that removal of SFTs is associated with simultaneous dislocation glide and climb. Jogs of atomic dimensions are formed when a fraction of SFT vacancies are absorbed by pipe diffusion. The width of a flow channel is explained in terms of two length scales: the size of an individual SFT, and the dislocation source-to-boundary distance (d of the order of micrometres). While dislocation segments climb by a few atomic planes with each SFT destruction event, d determines the total number of such events. Numerically computed channel widths (about 70–150 nm), and the magnitude of radiation hardening in copper are consistent with experimental observations.

§1. INTRODUCTION

Many experimental observations have shown that neutron irradiation of metals and alloys at temperatures below recovery stage V causes a substantial increase in the upper yield stress (radiation hardening) and, beyond a certain dose level, induces a yield drop and plastic instability (for example Smidt (1970), Dai (1995), Singh *et al.*

† Email: ghoniem@ucla.edu

(1996) and Baluc *et al.* (1999)). Furthermore, the post-deformation microstructure of a specimen showing the upper yield point has demonstrated two significant features. First, the onset of plastic deformation is generally found to coincide with the formation of 'cleared' channels, where almost all plastic deformation takes place. The second feature refers to the fact that the material volume in between cleared channels remains almost undeformed (i.e. no new dislocations are generated during deformation). In other words, the initiation of plastic deformation in these irradiated materials occurs in a very localized fashion. This specific type of plastic flow localization is considered to be one of many possibilities of plastic instabilities in both irradiated and unirradiated materials (for example Kocks *et al.* (1975), Neuhäuser (1990) and Luft (1991)).

A theory of radiation hardening was proposed by Seeger (1958) in terms of dislocation interaction with radiation-induced obstacles (referred to as *depleted zones*). Subsequently, Foreman (1968) performed computer simulations of loop hardening, in which the elastic interaction between the dislocation and loops was neglected. The model is based on Orowan's mechanism, which assumes that the obstacles are indestructible. In this view of matrix hardening, the stress necessary to overcome localized interaction barriers represents the increase in the yield strength, while long-range elastic interactions are completely ignored. These short-range dislocation-barrier interaction models lead to an estimate of the increase in the critical resolved shear stress (CRSS) of the form $\Delta\tau = \alpha\mu b/l$, where α is a numerical constant representing obstacle strength, μ is the shear modulus, b is the magnitude of the Burgers vector and l is the average interobstacle distance. Kroupa and Hirsch (1964) and Kroupa (1966), on the other hand, viewed hardening as a result of the long-range elastic interaction between slip dislocations and prismatic loops. In their model of friction hardening, the force necessary to move a rigid straight dislocation on its glide plane past a prismatic loop was estimated. In these two classes of hardening models, *all* dislocation sources are assumed to be simultaneously activated at the yield point, and plastic deformation is assumed to be homogeneous throughout the material volume. Thus, they do not specifically address the physics of plastic flow localization.

Singh *et al.* (1997) introduced the concept of *stand-off distance* for the decoration of dislocations with small self-interested atom (SIA) loops and proposed the *cascade-induced source hardening* (CISH) model, in analogy with the atmosphere Cottrell (1948). Detailed elasticity calculations showed that glissile defect clusters that approach dislocation cores within the stand-off distance are absorbed, while clusters can accumulate just outside this distance (Ghoniem *et al.* 2000a). Singh *et al.* (1997) concluded that dislocation decoration is a consequence of defect cluster mobility and trapping in the stress field of grown-in dislocations. The CISH model was used to calculate the stress necessary to free decorated dislocations from the atmosphere of loops around them (upper yield, followed by yield drop), so that these freed dislocations can act as dislocation sources. The CRSS increase in irradiated copper was shown by Singh *et al.* (1997) to be given by $\Delta\tau \approx 0.1\mu(b/l)(d/y)^2$, where d and y are the defect diameter and stand-off distance respectively. Assuming that $y \approx d$, and that $l \approx 35b$, they estimated that $\Delta\tau/\mu \approx 0.5\%$. The phenomenon of yield drop was proposed to result from the unpinning of grown-in dislocations, decorated with small clusters or loops of SIAs. Figure 1 shows a set of stress-strain curves for annealed and cold-worked pure copper, copper containing a dispersion of aluminium oxide particles (also in cold-worked condition) and copper irradiated with

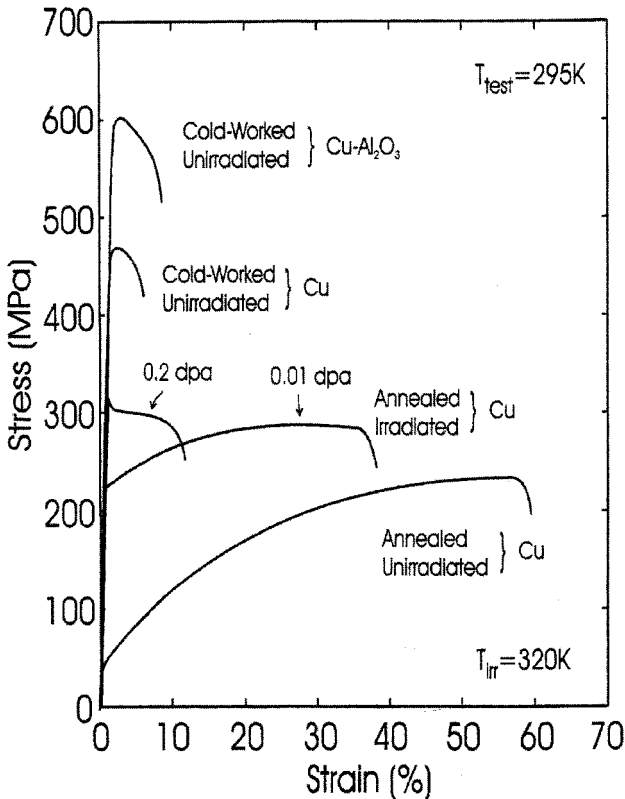


Figure 1. Experimental stress-strain curves for irradiated and unirradiated copper. Specimens were irradiated in the DR-3 reactor at Risø National Laboratory at 320 K, and tensile tested at 295 and 320 K (Singh *et al.* 1996).

fission neutrons at 320 K to dose levels of 0.01 and 0.2 displacements per atom (dpa), and tensile tested at 295 K (Singh *et al.* 1996). Neutron irradiation of pure copper at 320 K not only leads to an increase in the upper yield stress but also causes a prominent yield drop and plastic flow localization. An example of localized plastic flow in irradiated Cu-Cr-Zr alloy under low-cycle fatigue conditions is shown in figure 2. Note that cleared channels appear to be associated with relatively large inclusions (i.e. stress concentration).

The objective of the present study is to assess the physical mechanisms, which are responsible for the initiation of plastic instability in irradiated fcc metals by detailed numerical simulations of the interaction between dislocations and radiation-induced defect clusters. Two distinct problems that are believed to cause the onset of plastic instability are addressed in the present study. First, we aim at determining the mechanisms of dislocation unlocking from defect cluster atmospheres as a result of long-range elastic interaction between dislocations and sessile SIA clusters situated just outside the stand-off distance. The main new feature of this analysis is that dislocation deformation is explicitly considered during its interaction with SIA clusters. The results of this study are presented in § 3. Second, we investigate the mechanisms of structural softening in flow channels as a consequence of dislocation interaction with stacking-fault tetrahedra (SFTs). Based on these numerical simula-

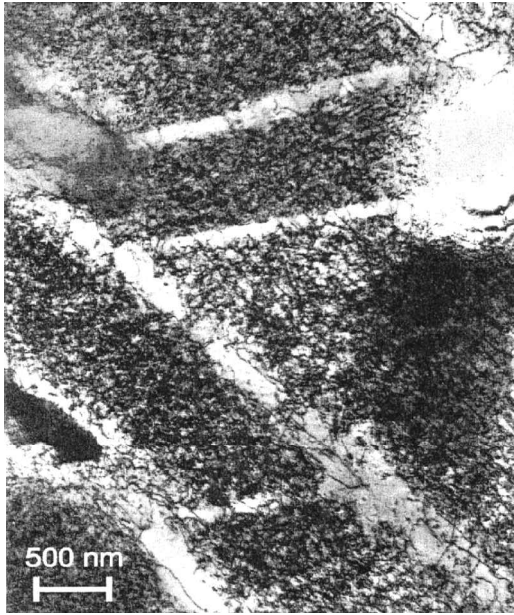


Figure 2. Transmission electron micrograph of localized plastic flow emanating from internal inclusions in Cu–Cr–Zr alloy, neutron irradiated at 320 K to a dose level of 0.3 dpa and fatigue tested at 320 K with a loading frequency of 0.5 Hz (Singh *et al.* 2000b).

tions, a new mechanism for the onset of channel formation is proposed, and the magnitude of radiation hardening is also computed in § 4. Finally, summary and conclusions are given in § 5.

§ 2. COMPUTATIONAL THREE-DIMENSIONAL DISLOCATION DYNAMICS

The method of dislocation dynamics has been recently developed for computer simulation of mesoscale plastic deformation. While the behaviour of single dislocations has been studied extensively in the past, complex dislocation ensemble interactions in three dimensions have not been attempted until recently (for example (Devincre and Condat (1992), Kubin and Canova (1992), Hirth *et al.* (1996), Schwarz (1997), Ghoniem and Sun (1999) and Ghoniem *et al.* (2000b)). In the following, we outline the main features of the parametric dislocation dynamics method for calculations of energies, stresses, forces and motion (Ghoniem and Sun 1999, Ghoniem *et al.* 2000b).

Slip dislocation loops emanating from Frank–Read (F–R) sources are each segmented into N_s segments (typically, N_s is in the range 7–30). Sessile SIA clusters, on the other hand, are assumed to be prismatic circular dislocation loops. Segments on F–R dislocations are parametrically described by the position vector components $\hat{r}_i(u)$:

$$\hat{r}_i(u) = \sum_{m=1}^{N_{DF}} \mathcal{C}_{im}(u)q_m, \quad (1)$$

where $\mathcal{C}_{im}(u)$ are shape functions, dependent on the parameter $u(0 \leq u \leq 1)$, q_m are generalized degrees of freedom (DOFs) for each node, and N_{DF} is the total number

of assigned DOFs. Equation (1) is a general parametric representation of the dislocation line for segment j . The velocity of any point on the dislocation line is \hat{r}_j ; $V_k = d\hat{r}_k/dt = \sum_{n=1}^{N_{DF}} C_{kn} dq_n/dt$. Curved segments of slip dislocations are represented by cubic splines. An efficient fast computational sum of the stress tensor components was developed by Ghoniem and Sun (1999):

$$\sigma_{ij} = \frac{\mu}{4\pi} \sum_{\gamma=1}^{N_{loop}} \sum_{\beta=1}^{N_s} \sum_{\alpha=1}^{Q_{max}} b_n w_\alpha \times \left(\frac{1}{2} R_{,mpp} (\varepsilon_{jmn} \hat{r}_{i,u} + \varepsilon_{imn} \hat{r}_{j,u}) \frac{1}{1-\nu} \varepsilon_{kmn} (R_{,ijm} - \delta_{ij} R_{,ppm}) \hat{r}_{k,u} \right), \quad (2)$$

where $R_{,ijk\dots}$ are successive derivatives of the radius vector connecting a point on the loop and a field point and ε_{kmn} is the usual permutation tensor. For a dislocation loop ensemble we use the property of linear superposition. Thus, the fast numerical sum is performed over the following set: quadrature points ($1 \leq \alpha \leq Q_{max}$) associated with weight factors w_α , loop segments ($1 \leq \beta \leq N_s$), and number of ensemble loops ($1 \leq \gamma \leq N_{loop}$). The parametric derivatives of the position vector are $\hat{r}_{k,u}$.

The elastic field of SIA clusters is computed using the infinitesimal loop approximation (Kroupa 1966): $\sigma_{ij} = k_{ij} \mu b R^2 / 2\rho^3$, where k_{ij} is an orientation factor of the order of unity, R is the loop radius and ρ is the distance from the loop centre. The total force and its moment on a SIA cluster can be expressed respectively as

$$F_i = -n'_j \sigma_{jk} b'_k \delta A' \quad (3)$$

and

$$M_i = -\varepsilon_{ijk} n'_j b'_l \sigma_{lk} \delta A', \quad (4)$$

where n'_j and $\delta A'$ refer to the Cartesian components of the normal vector and the habit plane area of the cluster respectively. As a mobile SIA dislocation loop moves closer to the core of the slip loop, the turning moment on its habit plane increases, as given by equation (4). When the mechanical work of rotation exceeds a critical value of 0.1 eV per crowdion (Foreman *et al.* 1992), we assume that the cluster changes its Burgers vector and habit plane and moves to be absorbed into the dislocation core. Thus, the mechanical work for cluster rotation is equated to a critical value (i.e. $\delta W = \int_{\theta_1}^{\theta_2} M_i d\theta_i = \Delta U_{crit}$) and used as a criterion to establish the stand-off distance (Ghoniem *et al.* 2000a).

We describe dislocation motion by developing equations of motion for generalized DOFs on the basis of a variational principle for Gibbs free energy, derived from irreversible thermodynamics. Inertial effects (i.e. the kinetic energy of moving dislocations) are not included in this work. We define the following:

- (i) $B_{\alpha k}$ as a diagonal friction (inverse mobility) matrix for phonon drag constants in two glide and one climb directions;
- (ii) the sum of the Peach–Kohler force, self-force, Peierls lattice friction and climb forces (per unit dislocation line length) as f'_k ;
- (iii) an effective *generalized force* f_m on a curved segment as

$$f_m = \int_0^1 f'_i C_{im}(u) |d\mathbf{s}|; \quad (5)$$

(iv) a phonon drag coefficient matrix element γ_{mn} as

$$\gamma_{mn} = \int_0^1 c_{im}(u) B_{ik} C_{kn}(u) |d\mathbf{s}|. \quad (6)$$

With these quantities calculated for each curved segment, Ghoniem *et al.* (2000b) showed that the global DOFs Q_l for the entire loop can be obtained by solving the set of differential equations given by

$$\mathcal{F}_k = \sum_{l=1}^{N_{\text{tot}}} \Gamma_{kl} Q_{l,t}. \quad (7)$$

Similar to the finite-element procedure, the local segment phonon drag coefficient matrix $[\gamma_{mn}]$ is added to the corresponding global locations in the phonon drag coefficient matrix $[\Gamma_{kl}]$, while the force vector is mapped on to a corresponding global vector \mathcal{F}_k . Here, the total number of DOFs for the loop are $N_{\text{tot}} = N_s N_{\text{DF}}$. The component Γ_{kl} is zero if the DOFs k and l are not connected through a segment. Equation (7) represents a set of time-dependent ordinary differential equations which describe the motion of dislocation loops as an evolutionary dynamical system. The computational time step is dictated by the dislocation mobility, which is quite high in fcc metals (the phonon drag coefficient in copper is taken as 5×10^{-5} Pa s (Kubin 1993)). Numerical integration of the equations of motion are performed by implicit iterative methods.

§ 3. UNLOCKING OF FRANK–READ SOURCES FROM CLUSTER DECORATIONS

The two main aspects considered here to affect both hardening and the ensuing plastic flow localization are

- (i) dislocation unlocking from defect cluster atmospheres and
- (ii) destruction of SFTs on nearby slip planes by gliding dislocations.

The interaction between grown-in dislocations and trapped defect clusters has been shown to lead to unfauling of vacancy clusters in the form of vacancy loops (Ghoniem *et al.* 2000a). It can also result in rotation of the habit plane of mobile SIA clusters (equation (4)). Once either of these two possibilities is realized for a vacancy or SIA cluster, it is readily absorbed into the dislocation core. Ghoniem *et al.* (2000a) used these conditions to determine an appropriate stand-off distance from the dislocation core, which is free of irradiation-induced defect clusters. It is estimated (Ghoniem *et al.* 2000a) that clusters within a distance of 3–9 nm from the dislocation core in copper will be absorbed, either by rotation of their Burgers vector or by unfauling. We shall use this estimate in § 3 as a guide to calculations of long-range interactions of dislocations with sessile prismatic SIA clusters situated outside the stand-off distance. While the experimentally observed average SFT size is about 2.5 nm for oxygen-free high-conductivity (OFHC) copper, the radius of a sessile interstitial cluster, which results from coalescence of smaller mobile clusters, is assumed to be in the approximate range 4–20 nm. We assume here that SIA cluster coalescence outside the stand-off distance leads to their immobilization because the resultant Burgers vector is outside the glide cylinder of coalesced SIA loops (Singh *et al.* 1997). The local density of interstitial defect clusters at the stand-off distance is taken to be in the range $(0.6\text{--}4) \times 10^{24} \text{ m}^{-3}$, giving an average intercluster spacing of

about $(18-35)a$. In subsequent computer simulations, we use the following set of material data for copper: lattice constant $a = 0.3615$ nm, shear modulus $\mu = 45.5$ GPa, Poisson's ratio $\nu = 0.35$ and F-R source length $L = (1500-2000)a$.

3.1. Interaction between a Frank-Read source and a single self-interstitial atom

To gain insight into the mechanism of dislocation unlocking from the elastic field of decorating clusters, we first consider the interaction between a F-R source and one single sessile SIA cluster (radius, $40a$) at a stand-off distance of $40a$ from the glide plane. The original analysis of Kroupa (1966) of a similar problem considered the case of a single straight, infinitely long and rigid dislocation, interacting with another single circular dislocation loop. More recently, Kubin and Kratochvil (2000) have analysed the interaction between an infinite dislocation and a rectangular dipolar loop.

In the following, the defect cluster is assumed to be a circular prismatic dislocation loop situated above (or below) the glide plane of a F-R source. The Burgers vector of clusters is $\mathbf{b} = \frac{1}{2}[110]$ or $\mathbf{b} = \frac{1}{2}[\bar{1}\bar{1}0]$ while, for the expanding F-R source, $\mathbf{b} = \frac{1}{2}[\bar{1}01]$. Other equivalent cluster orientations give redundant results. We also assume here that the dislocation loop is not dissociated into partials. A uniaxial stress along $[100]$ of $\sigma_{11} = 100$ MPa is suddenly applied. The equations of motion for position and tangent vectors are solved for 21 nodes on the expanding source, and the shape is recomputed by implicit iterative integration to ensure stability of the solution. Figure 3 shows a projection on the (111) glide plane of the change in shape

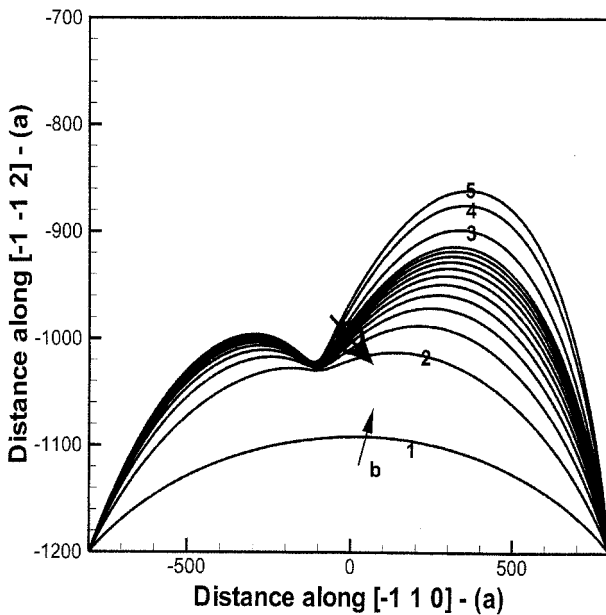


Figure 3. Dynamics of F-R source ($\mathbf{b} = \frac{1}{2}[\bar{1}01]$) interaction with a single sessile prismatic interstitial defect cluster near the glide plane. The cluster has a radius of $50a$, and a Burgers vector $\mathbf{b} = \frac{1}{2}[110]$. The cluster is located at $(0, -1000a, 40a)$ in the local glide plane coordinates. Time intervals are as follows: curve 1, 1 ps; curve 2, 2.5 ps; curve 3, 25 ps; curve 4, 50 ps; curve 5, 1200 ps.

for the expanding F–R source dislocation, as it comes closer to the cluster location. After 1 ps, the advancement of the F–R source is nearly unaffected by the prismatic defect cluster off the glide plane, as shown in figure 3. As the dislocation line of the F–R source comes within $(100\text{--}200)a$ of the cluster, it is repelled and starts to deform significantly by about 25 ps. Even though the cluster force is relatively small, the dislocation line is very flexible, thus achieving an equilibrium configuration in about 0.1 ns. When the same sessile SIA cluster is moved vertically away from the glide plane, the interaction dynamics are significantly changed, both quantitatively and qualitatively (figure 4). By about 10 ps, the F–R source dislocation clears itself from the influence of the cluster force field, which just distorts the dislocation line as it passes underneath it on the glide plane. The line deformation caused by the cluster is eventually erased as a result of the restoring dislocation self-force. It is clear that the F–R source dislocation unlocks itself rather easily and quickly from the elastic field of one single SIA cluster at a distance of $80a$ from the glide plane. In both cases studied here, the greatest influence of the cluster on the dislocation line distortion is shifted from the minimum (stand-off) distance between them. This shift is a consequence of the specific Burgers vector orientations of both the SIA cluster and the F–R source dislocation. The cluster force F_c on the F–R dislocation line, projected along its normal \mathbf{n} on the glide plane, can be shown to be given by $F_c \mathbf{n} = -(\sigma_{3i} b_i) \mathbf{n}$, the magnitude of which is dependent on the cluster's Burgers vector through σ_{3i} and

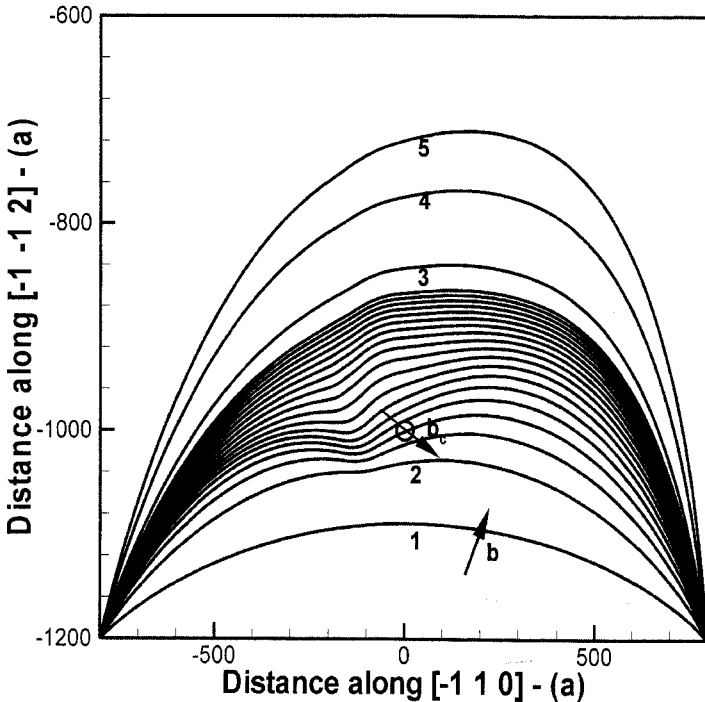


Figure 4. Dynamics of F–R source interaction with a single sessile prismatic interstitial defect cluster at a larger stand-off distance. All conditions are the same as in figure 3, except that the cluster is located at $(0, -1000a, 80a)$ in the local glide plane coordinate, and time intervals are as follows: curve 1, 1 ps; curve 2, 2.5 ps; curve 3, 25 ps; curve 4, 50 ps; curve 5, 75 ps.

the F–R line Burgers vector components b_i . In the specific case when $\mathbf{b} = \frac{1}{2}[\bar{1}01]$, this force magnitude is proportional to the difference between the cluster's normal stress σ_{33} and its shear stress σ_{31} , which maximizes at a position shifted from the minimum stand-off distance. When this is considered in the dynamics of the advancing line, a clear shift in the maximum cluster influence is produced, as can be seen in figures 3 and 4.

3.2. Interaction between a Frank–Read source and a row of self-interstitial atom clusters

Consider now the more complex interaction between an expanding F–R source dislocation and the full field of multiple sessile SIA clusters (loops) present in a region of decoration. As the F–R source expands in the elastic field of SIA clusters, each point on the dislocation line will experience a resistive (or attractive) force, which must be overcome for the dislocation to move further. The dislocation line curvature and hence the local self-force also change dynamically. To determine the magnitude of collective cluster resistance, systematic calculations for the dynamics of interaction between attractive (figure 5) and repulsive (figure 6) SIA clusters are presented. When the SIA clusters are all attractive, the dislocation line is immediately pulled into their atmosphere but, as the applied stress is increased, the dislocation remains trapped by the force field of SIA clusters. When the stress is increased to 200 MPa, the line develops an asymmetric configuration as a result of its Burgers vector orientation, and an unzipping instability eventually unlocks the F–R source from the collective cluster atmosphere, as shown in figure 5. This asymmetric unlock-

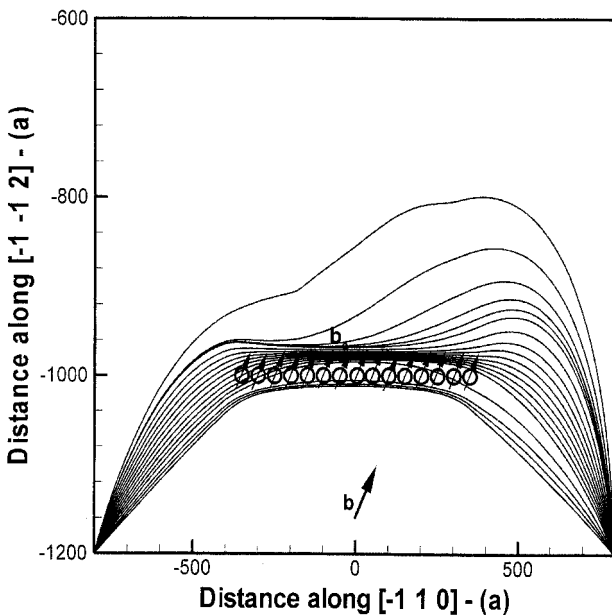


Figure 5. Dynamics of F–R source interaction with a row of attractive SIA clusters at a stand-off distance of $40a$. Clusters have parallel and identical Burgers vectors to the F–R source of $\mathbf{b} = \frac{1}{2}[\bar{1}01]$, and their centres are separated by $50a$. The applied stress σ_{11} is gradually increased to 200 MPa before the dislocation line breaks free from the clusters.

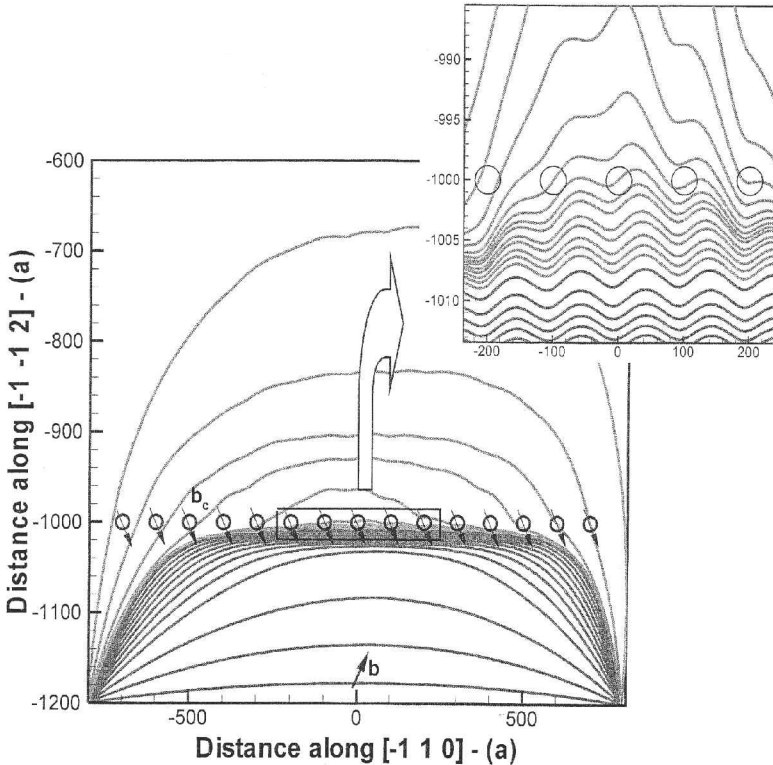


Figure 6. Dynamics of a fluctuation-induced morphological instability initiated when the dislocation line passes near the cluster atmosphere. The conditions are the same as in figure 5, except that the clusters are repulsive with $\mathbf{b} = \frac{1}{2}[110]$.

ing mode is characteristic of high linear cluster density on smaller sections of F–R source decorations, as shown in figure 5, where the linear density of SIA clusters is about $\frac{1}{50}$ (cluster/lattice constant). On the other hand, as the linear density of SIA clusters is reduced to about $\frac{1}{100}$ (cluster/lattice constant), and the cluster coverage of the F–R source is extensive, another instability mode develops. Figure 6 shows the detailed dynamics of the collective cluster interaction with an expanding F–R source. The high fidelity of the current parametric dislocation dynamics method for space and time resolution of this interaction is clearly shown in the inset to figure 6. A fluctuation in the line shape is amplified by the combined effects of the applied and self-forces on the middle section of the F–R source, and the dislocation succeeds in penetrating through the collective cluster field at a critical tensile stress of $\sigma_{11} = 200$ MPa (CRSS $\tau/\mu = 0.18\%$). A summary set of results for repulsive clusters of parallel Burgers vectors are shown as scaling graphs in figures 7 and 8. The CRSS τ/μ is shown in figure 7 as a function of the stand-off distance, for a fixed intercluster distance of $50a$. The results of current calculations are compared with the analytical estimates of Singh *et al.* (1997) and Trinkaus *et al.* (1997b). For larger stand-off distances, the current results show a larger critical stress compared with the analytical estimates, while for stand-off distances smaller than about $60a$, a smaller critical stress is required to unlock the F–R source. When the stand-off distance is large, the applied stress must overcome the self-force, which results from the finite length of the

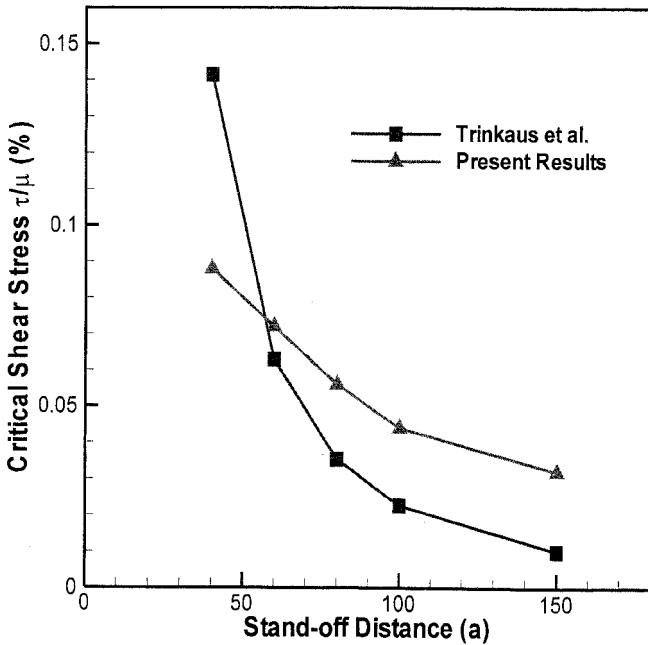


Figure 7. Scaling of the critical shear stress with the stand-off distance for repulsive clusters of parallel $\mathbf{b} = \frac{1}{2}[110]$ at fixed intercluster spacing of $50a$.

F–R source, in addition to the collective cluster elastic field. This aspect is not considered in the extension made by Trinkaus *et al.* (1997b) to Kroupa's (1966) theory, where the line is assumed to be rigid as it moves close to the clusters. At smaller stand-off distances, however, the dislocation easily unlocks by one of the two instability modes discussed earlier, and the predicted CRSS is smaller than analytical estimates. Similar features are displayed in figure 8, where our calculations are again compared with the analytical scaling relationship developed by Trinkaus *et al.* (1997b). The nature of the clusters' elastic field, whether attractive or repulsive, influences the magnitude of the CRSS, which is found to be higher for attractive (figure 5) as opposed to repulsive (figures 7 and 8) elastic fields.

It is estimated that the required CRSS is about 0.1% of μ (about 50 MPa for copper), for an average intercluster distance $l \approx 50a$, and a stand-off distance of about $40a$. It is experimentally difficult to determine the local value of l in the decoration region of dislocations, which is likely to vary considerably, depending on the character of the dislocation Burgers vector. However, $l \approx 50a$ is an upper bound, while $l \approx (20\text{--}30)a$ is more likely. Since the CRSS is roughly inversely proportional to l , the most likely value of the CRSS to unlock dislocations and to start the operation of F–R sources would be $\tau_{\text{CRSS}} \approx 100\text{--}150$ MPa. Depending on the local value of the Schmid factor, the corresponding uniaxial applied stress is thus likely to be of the order of 200–300 MPa, under conditions of heavy decoration (i.e. at a displacement damage dose of 0.1 dpa or more). The current estimates for the unlocking stress are thus consistent with the experimental data in figure 1 and indicate that the operation of F–R sources from decorated dislocations can be initiated by one (or both) of the following possibilities.

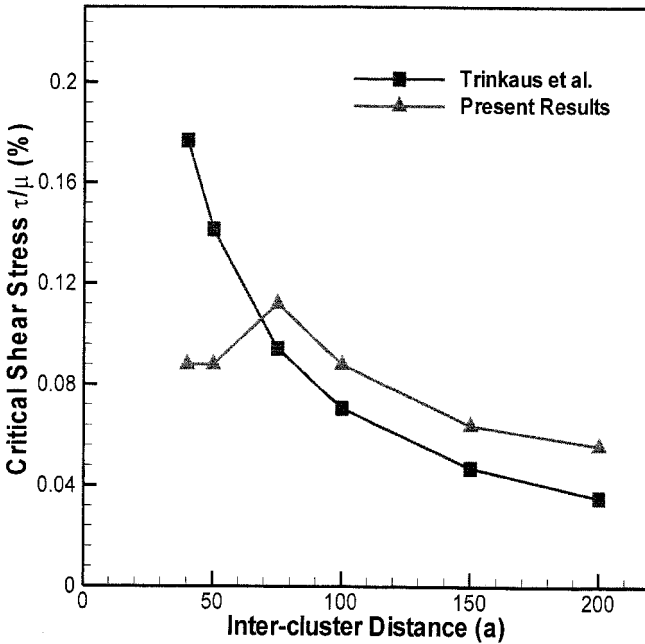


Figure 8. Scaling of the critical shear stress with the intercluster distance for repulsive clusters of parallel $\mathbf{b} = \frac{1}{2}[110]$, at a fixed stand-off distance of $40a$.

- (i) Activated F–R sources are decorated with a statistically low linear defect cluster density.
- (ii) Dislocation sources are initiated at stress singularities in regions of internal stress concentration.

In either of these two possibilities, the most likely orientation of plastic slip is along directions of maximum local Schmid factors.

§4. INTERACTION BETWEEN DISLOCATIONS AND STACKING-FAULT TETRAHEDRA AND THE MECHANISM OF CHANNEL FORMATION

Once dislocation sources are unlocked from their decoration atmospheres causing a yield drop, they additionally interact with the surrounding random field of defect clusters (e.g. vacancy loops or SFTs). We investigate here the interaction between emitted F–R dislocations and vacancy-type defect clusters as a possible mechanism of radiation softening immediately beyond the yield point. Numerical computer simulations are performed for the penetration of undissociated slip dislocation loops emitted from active F–R sources (i.e. unlocked from defect decorations) against a random field of SFTs or sessile Frank loops of the type: $\frac{1}{3}\langle 111 \rangle\{111\}$. At the present level of analysis, we do not distinguish between SFTs and vacancy loops, since they are modelled as point obstacles to dislocation motion that can be destroyed once an assumed critical force on them is reached. The long-range elastic field of these obstacles is ignored. The present computer simulations are extensions of Foreman's (1968) analysis in the following respects.

- (i) Dislocation sources are not free segments and are emitted from pinned F–R sources.
- (ii) The simulations are fully three dimensional (3D) and not on a single glide plane.
- (iii) Obstacles are destructible, a necessary condition for flow localization.
- (iv) Multiple 3D jogged and interacting dislocation loop pile-ups are simulated.
- (v) Dislocation segments in between SFTs are *not* in equilibrium with the applied stress.

The random distribution of SFTs is generated as follows.

- (i) The volumetric density of SFTs is used to determine the average 3D position of each generated SFT.
- (ii) A Gaussian distribution function is used (with the standard deviation being 0.1–0.3 of the average spacing) to assign a final position for each generated SFT around the mean value.
- (iii) The intersection points of SFTs with glide planes are computed by finding all SFTs that intersect the glide plane.

For simplicity, we perform this procedure assuming that SFTs are spherical and uniform in size.

4.1. Interaction between unlocked dislocations and stacking-fault tetrahedra

First, one slip dislocation loop is introduced between two fixed ends, as in § 3. A search is then performed for all neighbouring SFTs on the glide plane. Subsequent nodal displacements (governed by the local velocity) are adjusted such that a released segment interacts with only one SFT at any given time. The interaction scheme is a dynamic modification of Friedel (1956) statistics, where the asymptotic maximum plane resistance is found by assuming steady-state propagation of quasistraight dislocation lines. While Friedel calculated the area swept as the average area per particle on the glide plane, we adjust the segment line shape dynamically over several time steps after it is released from a SFT. When a segment is within $5a$ of the centre of any SFT, it is divided into two segments with an additional common node at the point of SFT intersection with the glide plane. The angle between the tangents to the two dislocation arms at the common node is then computed, and force balance is performed. When the angle between the two tangents reaches an assumed critical value Φ_c , the node is released, and the two open segments are merged into one. If the force balance indicates that the segment is near equilibrium, no further incremental displacements of the node are added, and the segment of the loop is temporarily stationary. However, if a net force acts on that segment of the loop, it is advanced and the angle recomputed. The angle between tangents may reach the critical value, even though the segment is not in equilibrium.

Sun *et al.* (2001) have shown that the elastic interaction energy between a glissile dislocation and a SFT is not sufficient to transform the SFT into a glissile prismatic vacancy loop. They proposed an alternate mechanism for the destruction of SFTs by passage of jogged and/or decorated dislocations close to the SFT. The energy released from recombination of a small fraction of vacancies in the SFT was estimated to result in its local rearrangement. In the present calculations, we assume that vacancies in the SFT are absorbed in the dislocation core of the small contacting dislocation segment, forcing it to climb and form atomic jog pairs. With this

mechanism, the entire SFT is removed from the simulation space, and dislocations continue to glide on separate planes, thus dragging atomic-size jogs with them. Successive removal of SFTs from nearby glide planes can lead to channel formation and flow localization in the channel, because the passage of consecutive dislocation loops emitted from the F–R source is facilitated with each dislocation loop emission. Figure 9 shows the results of computer simulations for propagation of plastic slip emanating from a single F–R source in copper irradiated and tested at 100°C (Singh *et al.* 2000a). The density of SFTs is $4.5 \times 10^{23} \text{ m}^{-3}$ and the average size is 2.5 nm. In this simulation, the crystal size is set at about $1.62 \mu\text{m}$, while the initial F–R source length is $1600a$ (about 576 nm). A uniaxial applied tensile stress σ_{11} along [100] is incrementally increased, and the dislocation line configuration is updated until equilibrium is reached at the applied stress. Once full equilibrium of the dislocation line is realized, the stress is increased again, and the computational cycle repeated. At a critical stress level (flow stress), the equilibrium dislocation shape is no longer sustainable, and the dislocation line propagates until it is stopped at the crystal boundary, which we assume to be impenetrable. All SFTs interacting with the dislocation line are destroyed, and plastic flow on several closely spaced glide planes is only limited by dislocation–dislocation interaction through the pile-up mechanism.

During the initial stages of deformation, small curved dislocation segments unzip, forming longer segments that are stuck until they are unzipped again by increasing the applied stress. As a result of the higher stiffness of screw dislocation segments compared with edge components, the F–R source dislocation elongates

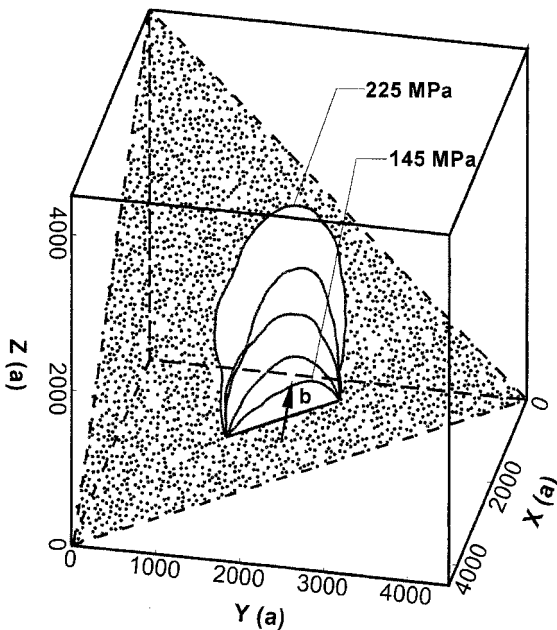


Figure 9. Propagation of plastic slip emanating from a single F–R source in copper irradiated and tested at 100°C (displacement damage dose, 0.1 dpa; SFT density $4.5 \times 10^{23} \text{ m}^{-3}$; size, 2.5 nm; simulated crystal size, $4500a$ ($1.62 \mu\text{m}$); initial F–R source length, $1600a$ (576 nm); stress applied along [100]).

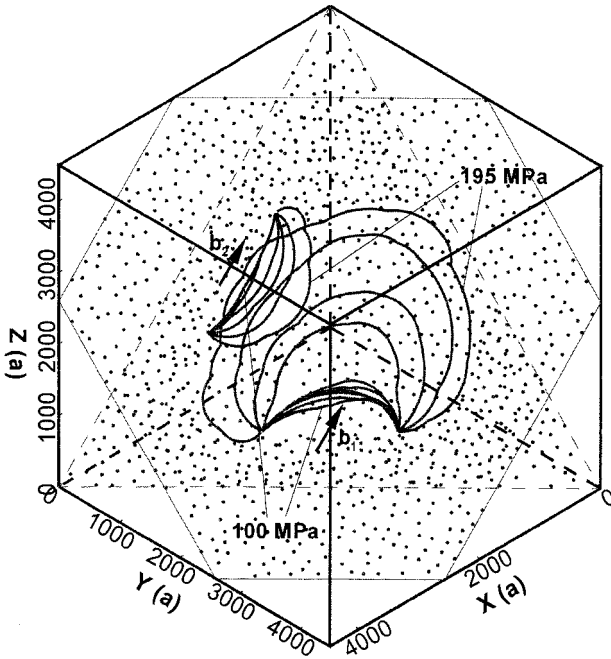


Figure 10. Spread of plastic slip emanating from two interacting F-R sources in copper irradiated and tested at 100°C. While the simulation conditions are the same as in figure 9, the two F-R sources are separated by $20a$ (7.2 nm).

along the direction of its Burgers vector. The final configuration, however, is determined by

- the character of its initial segment (e.g. screw or edge),
- the distribution of SFTs intersecting the glide plane and
- dislocation-dislocation interactions.

This aspect is illustrated in figure 10, where two interacting F-R sources in copper are shown for a displacement dose of 0.01 dpa and a SFT density of $2.5 \times 10^{23} \text{ m}^{-3}$ and with an average size of 2.5 nm. All other conditions are the same as in figure 9. The two F-R sources are separated by $20a$ (about 7.2 nm). It is seen that the spread of the F-R dislocation line with an initial strong edge component of the Burgers vector is much faster than the F-R source with an initial pure screw component. Significant deformation of the two loops is also observed when corresponding segments meet, and a higher stress is required to overcome additional interaction forces.

4.2. Matrix radiation hardening

Penetration of activated F-R sources into a 3D field of destructible SFTs can be viewed as a percolation problem, first considered by Foreman (1968) on a single glide plane and extended here to complex 3D climb-controlled glide motion. The critical stress above which an equilibrium dislocation configuration is unsustainable corresponds to the percolation threshold and is considered here to represent the flow stress of the radiation-hardened material. The effects of interplanar F-R source

interactions on the flow stress in copper irradiated and tested at 100°C are shown in figure 11. A plastic stress–strain curve is constructed from the computer simulation data, where the local strain is measured in terms of the fractional area swept by expanding F–R sources on the glide plane. It is shown that, while the majority of the increase in applied stress of irradiated copper can be rationalized in terms of dislocation interaction with SFTs on a single glide plane, dislocation–dislocation dipole hardening can have an additional small component of the order of 15% for very close dislocation encounters on neighbouring slip planes (e.g. separated by about $20a$). For larger separations (e.g. about $500a$) the additional effects of dipole hardening is negligible. Dislocation forest hardening does not seem to play a significant role in determination of the flow stress, as implicitly assumed in earlier treatments of radiation hardening (for example Seeger (1958), Makin and Minter (1960) and Foreman (1968)). The influence of the irradiation dose on the local stress–strain behaviour of copper irradiated and tested at 100°C is shown in figure 12 for $\Phi_c = 165^\circ$. In the present calculations, we do not consider strain hardening by dislocation–dislocation interaction and make no attempt to reproduce the global stress–strain curve of irradiated copper. Computed values of the flow stress are in general agreement with the experimental measurements of Singh *et al.* (2000a, 2001), as can be seen from figure 13. Closer agreement with experimental data depends on the value of the critical interaction angle Φ_c , which is the only relevant adjustable parameter in the present calculations. Determination of the two adjustable parameters Φ_c and B requires atomistic computer simulations beyond the scope of the present investigation. Additional calculations for the flow stress for OFHC copper, irradiated at 47°C and tested at 22°C are given in table 1 and compared with the experimental data of Singh *et al.* (1996). The flow stress value at a dose of

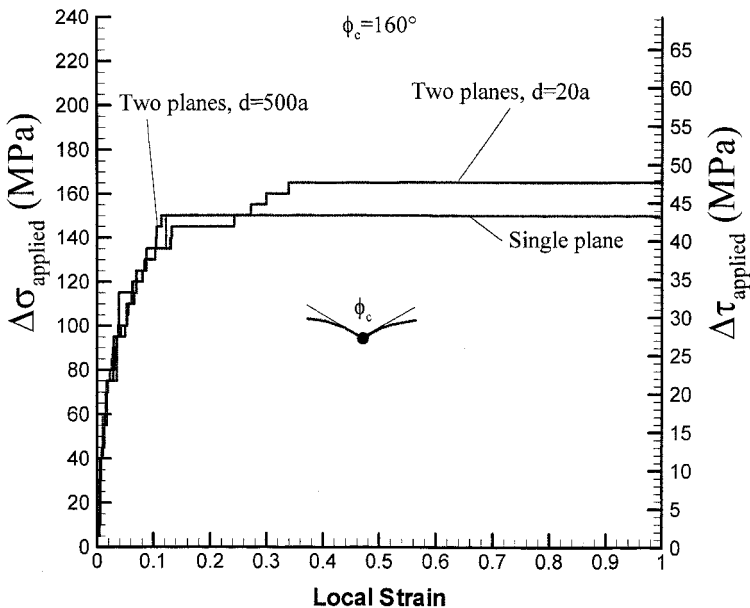


Figure 11. The effects of interplanar F–R source interactions on the flow stress in copper irradiated and tested at 100°C , and a displacement damage dose of 0.1 dpa. Local strain is measured as the fractional area of swept glide planes.

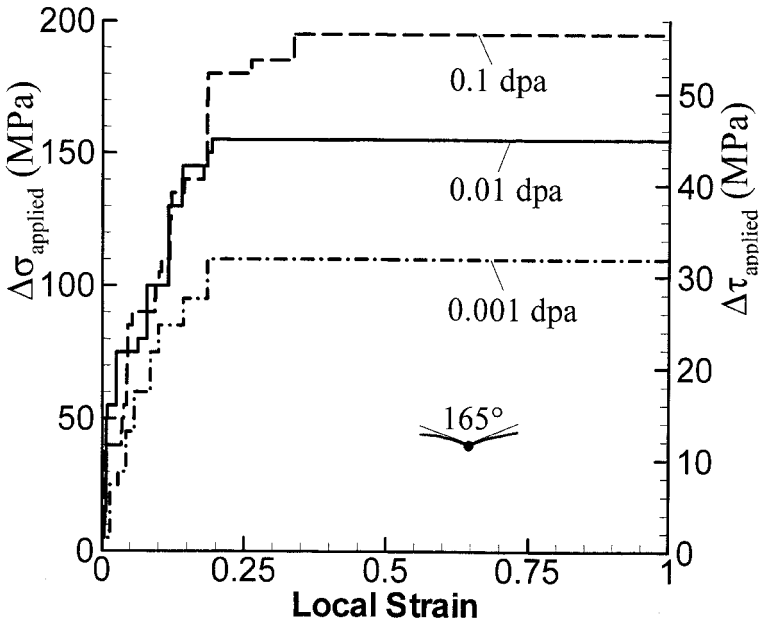


Figure 12. Dose dependence of the increase in flow stress in copper irradiated and tested at 100°C. The displacement damage dose varies in the range 0.001–0.1 dpa, and the conditions correspond to the experimental data of Singh *et al.* (2000a, 2001).

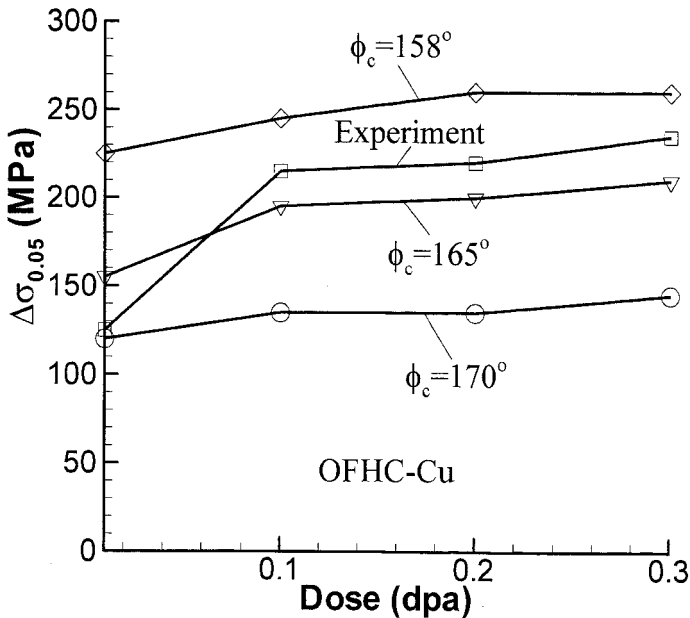


Figure 13. Comparison between the dose dependence of computed increase in flow stress values and the experimental measurements of Singh *et al.* (2000a, 2001).

Table 1. Experimental (Singh *et al.* 1996) and calculated tensile hardening parameters for OFHC copper, irradiated at 47°C and tested at 22°C.

Displacement dose (dpa)	SFT density (10^{23} m^{-3})	Planar inter-SFT distance a	Experimental $\Delta\sigma_{0.05}$ (MPa)	Calculated $\Delta\sigma$ (MPa)	
				$\Phi_c = 160^\circ$	$\Phi_c = 165^\circ$
0.001	0.8	196	110 ^a	145	110
0.01	5.3	76	134	240	205
0.1	6.7	67.5	238	250	210
0.2	6.6	68.5	249	245	205

^a From Dai (1995).

0.001 dpa has been extrapolated from the experimental results of Dai (1995) for single-crystal copper irradiated with 600 MeV protons. It is noted that, while the general agreement between the computer simulations and the experimental data of irradiated copper is reasonable at both 22 and 100°C, the dose dependence of radiation hardening indicates that some other mechanisms may play a role in radiation hardening.

4.3. Mechanism of channel formation

Investigations of dislocation interaction with full or truncated SFTs considered recently by Sun *et al.* (2001) indicated that local heating may be responsible for the dissolution of SFTs by interacting dislocations and that their vacancy contents are likely to be absorbed by rapid pipe diffusion into the dislocation core. The consequence of this event is dislocation climb out of its glide plane by the formation of atomic jogs, followed by subsequent glide motion of jogged dislocation segments on a neighbouring plane. In figure 14, we present results of computer simulations of the climb-controlled glide mechanism of jogged F–R source dislocations. Figure 15 shows a side view of the climb-controlled glide motion of a dislocation loop pile-up, consisting of three successive loops, by projecting dislocation lines on the plane formed by the vectors $[111]$ and $[\bar{1}\bar{1}2]$. SFTs have been removed for clarity of visualization. It is noted that, for this simulated three-dislocation pile-up, the first loop reaches the boundary and is held there while the second and third loops expand on different slip planes. We assume that the simulation boundary is rigid, with no attempt to simulate slip transmission to neighbouring grains. However, the force field of the first loop stops the motion of the second and third loops, even though the stress is sufficient to penetrate through the field of SFTs. This climb-controlled glide mechanism of jogged dislocations in a pile-up can be used to explain two aspects of dislocation channel formation. As the group of emitted dislocations expand by glide, their climb motion is clearly determined by the size and density of SFTs. The climb distance is computed from the number of vacancies in a SFT distributed over the length of contacting dislocation segments. The jog height is thus variable but is generally of atomic dimensions for the conditions considered here.

As a consequence of this climb-controlled glide mechanism, the width of the channel is a result of two length scales: firstly, the average size of a SFT (about 2.5 nm) and, secondly, the F–R source-to-boundary distance (about 1–10 μm). This aspect can be seen from figure 2. Secondary channels, which are activated from a primary channel (i.e. source point) and which end up in a nearby primary channel

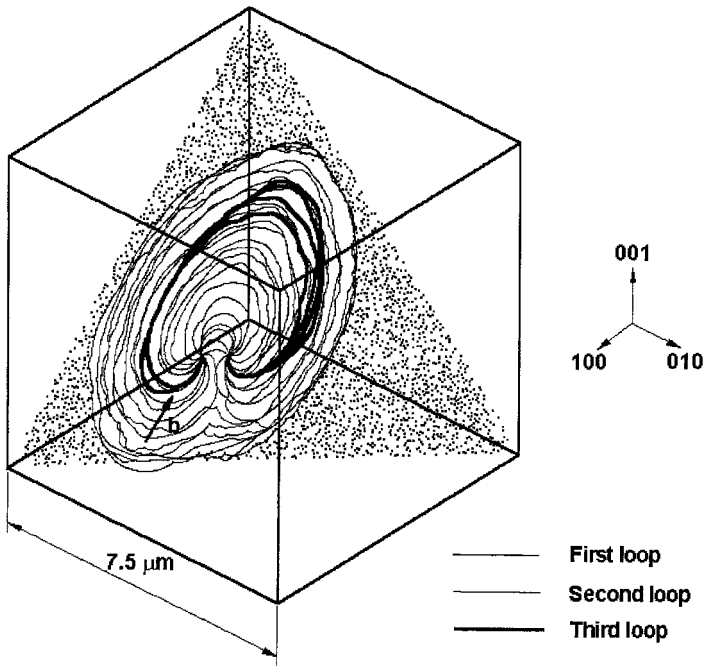


Figure 14. A front 3D view of the glide-controlled climb mechanism for a jogged dislocation pile-up. Note the gradual destruction of SFTs as the pile-up develops.

(i.e. boundary), are thinner than primary channels. Further detailed experimental observations of the channel width dependences are necessary before final conclusions can be drawn. The second aspect of experimental observations (figure 1), which can also be explained by the present mechanism, is that a small degree of hardening occurs once dislocation channels have been formed. Dislocation–dislocation interaction within the non-coplanar jogged pile-up requires a higher level of applied stress to propagate the pile-up into neighbouring grains. While the initiation of a dislocation channel is simulated here, full evolution of the channel requires successive activation of F–R sources within the volume weakened by the first F–R source, as well as forest hardening within the channels themselves.

The possibility of dislocation channel initiation on the basis of the climb-controlled glide mechanism is further investigated by computer simulation of OFHC copper irradiated to 0.01 dpa and tested at 100°C; this is shown in figure 16. The figure is a 3D representation of the initial stages of multiple-dislocation-channel formation. For clarity of visualization, the apparent SFT density has been reduced by a factor of 100, since the total number of SFTs in the simulation volume is 3.125×10^7 . The initial dislocation density is taken as $\rho = 10^{13} \text{ m}^{-3}$. To demonstrate the importance of spatial SFT density variations, a statistical spatial distribution within the simulation volume has been introduced such that lower SFT densities are assigned near ten glide planes. All dislocation segments are inactive as a result of the high local SFT density, except for those on the specified glide planes. Search for nearby SFTs is performed only close to active channel volumes, which in this case totals 174 846. It is observed that, within a $5 \mu\text{m}$ volume, the number of loops within a pile-up does not exceed five. It is expected that, if the pile-up continues across an

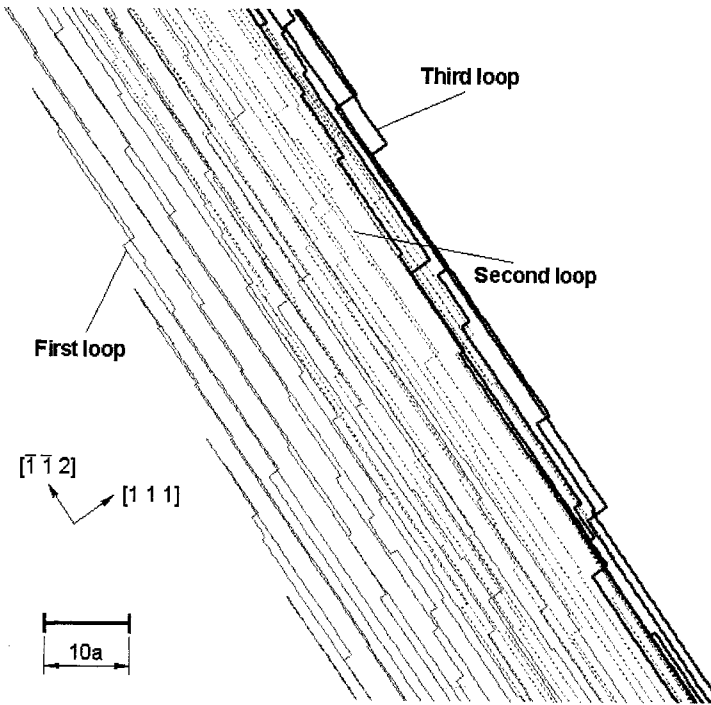


Figure 15. Side-view projection for glide-controlled climb motion of a dislocation loop pile-up on the plane spanned by the vectors $[111]$ and $[\bar{1}\bar{1}2]$ consisting of three successive loops. SFTs have been removed for clarity of visualization.

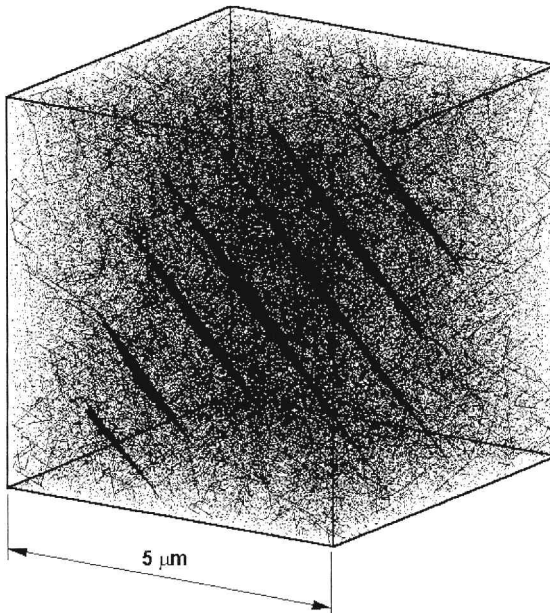


Figure 16. 3D view for the formation of dislocation channels on glide planes which have low SFT density, for irradiated copper at a dose of 0.01 dpa. For clarity of visualization, the apparent SFT density has been reduced by a factor of 100.

entire grain (size, about 10 μm), a higher number of loops would be contained in a jogged dislocation pile-up and that the corresponding channel would be wider than in the present calculations. We have not attempted to initiate multiple F–R sources within the volume swept by the dislocation pile-up to simulate the full evolution of channel formation. As a result, the channel shape created by a single active F–R source is of a wedge nature. In future simulations, we plan to investigate the full evolution of dislocation channels.

§ 5. SUMMARY AND CONCLUSIONS

The present investigations have shown that dislocation lines are highly flexible. For small intercluster or stand-off distances (which are typical of decorated dislocations), the unlocking stress varies by as much as a factor of two from the results of rigid dislocation interactions. Two possible mechanisms of dislocation unlocking have been identified: firstly, an asymmetric unzipping-type instability caused by partial decoration of dislocations; secondly, a fluctuation-induced morphological instability, when the dislocation line is extensively decorated by defect clusters. Estimated unlocking stress values are in general agreement with experimental observations that show a yield drop behaviour. It appears that unlocking of heavily decorated dislocations will be most prevalent in areas of stress concentration (e.g. precipitate, grain boundary, triple-point junction or surface irregularity).

Computer simulations for the interaction between unlocked F–R sources and a 3D random field of SFTs have been utilized to estimate the magnitude of radiation hardening, and to demonstrate a possible mechanism for the initiation of localized plastic flow channels. Reasonable agreement with experimental hardening data has been obtained with the critical angle Φ_c in the limited range 158–165°. Both the magnitude and the dose dependence of the increase in flow stress by neutron irradiation at 50 and 100°C are reasonably well predicted. In spatial regions of internal high stress, or on glide planes of statistically low SFT densities, unlocked dislocation sources can expand and interact with SFTs. Dislocations drag atomic-size jogs and/or small glissile SIAs when an external stress is applied. A high externally applied stress can trigger point-defect recombination within SFT volumes resulting in local high temperatures. A fraction of the vacancies contained in SFTs is therefore absorbed into the core of a gliding dislocation segment producing atomic-size jogs and segment climb. The climb height is a natural length scale dictated by the near-constant size of the SFT in irradiated copper. It is shown by the present computer simulations that the width of a dislocation channel is of the order of 200–500 atomic planes, as observed experimentally, and is a result of a stress-triggered climb-controlled glide mechanism. The atomic details of the proposed dislocation–SFT interaction and ensuing absorption of vacancies into dislocations need further investigations by atomistic simulations.

Finally, it should be pointed out that, at relatively high neutron doses, dense decorations of dislocations with SIA loops, and a high density of defect clusters and loops in the matrix are most likely to occur. As shown here, these conditions can lead to the phenomena of yield drop and flow localization. Solutions of these problems in the field of materials design may be sought, either to avoid dislocation decorations and channel formation, or to prevent propagation of dislocations through the channels (e.g. by providing closely spaced indestructible obstacles on glide planes).

ACKNOWLEDGEMENTS

Research is supported by the US Department of Energy, Office of Fusion Energy, grant DE-FG03-98ER54500, with University of California, Los Angeles, and is partially funded by the European Fusion Technology program. The authors would like to acknowledge the critical comments and reviews of this work by Dr Helmut Trinkaus and Dr Alan Foreman, and the computational assistance of Mr Jianming Huang.

REFERENCES

- BALUC, N., DAI, Y., and VICTORIA, M., 1999, *Proceedings of the 20th International Symposium on Metallurgy and Materials Science*, edited by J. B. Bilde-Sorensen, J. V. Cartensen, N. Hansen, D. Juul Jensen, T. Leffers, W. Pantleon, O. B. Pedersen and G. Winther (Risø: Risø National Laboratory).
- COTTRELL, A. H., 1948, *Report of a Conference on the Strength of Solids* (Bristol, London: Physical Society), p. 30.
- DAI, Y., 1995, PhD Thesis 1388, University of Lausanne, p. 59.
- DEVINCRE, B., and CONDAT, M., 1992, *Acta metall. mater.*, **40**, 2629.
- FRIEDEL, J., 1956, *Les Dislocations* (Paris: Gauthiers-Villiar).
- FOREMAN, A. J. E., 1968, *Phil. Mag.*, **17**, 353.
- FOREMAN, A. J. E., ENGLISH, C. A., and PHYTHIAN, W. J., 1992, *Phil. Mag.*, **66**, 655.
- GHONIEM, N. M., SINGH, B. N., SUN, L. Z., and DIAZ DE LA RUBIA, T., 2000a, *J. nucl. Mater.*, **276**, 166.
- GHONIEM, N. M., and SUN, L. Z., 1999, *Phys. Rev. B*, **60**, 128.
- GHONIEM, N. M., TONG, S.-S., and SUN, L. Z., 2000b, *Phys. Rev. B*, **61**, 913.
- HIRTH, J. P., RHEE, M., and ZBIB, H. M., 1996, *J. Comput. Aided Mater. Des.*, **3**, 164.
- KOCKS, U. F., ARGON, A. S., and ASHBY, M. F., 1975, *Prog. Mater. Sci.*, **19**, 1.
- KROUPA, F., 1966, *Theory of Crystal Defects*, edited by B. Gruber (Prague: Academia), p. 275.
- KROUPA, F., and HIRSCH, P. B., 1964, *Discuss. Faraday Soc.*, **38**, 49.
- KUBIN, L. P., 1993, *Phys. Status sol. (a)*, **135**, 433.
- KUBIN, L. P., and CANOVA, G., 1992, *Scripta metall.*, **27**, 957.
- KUBIN, L. P., and KRATOCHVIL, J., 2000, *Phil. Mag. A*, **80**, 201.
- LUFT, A., 1991, *Prog. Mater. Sci.*, **35**, 97.
- MAKIN, M. J., and MINTER, F. J., 1960, *Acta metall.*, **8**, 691.
- NEUHAÜSER, H., 1990, *Patterns, Defects and Materials Instabilities*, NATO Advanced Study Institute Series, Series E, Vol. 183, edited by D. Walgraef and N. M. Ghoniem (Dordrecht Kluwer), pp. 241–276.
- SCHWARZ, K. W., 1997, *Phys. Rev. Lett.*, **78**, 4785.
- SEEGER, A., 1958, *Proceedings of the Second UN International Conference on the Peaceful Uses of Atomic Energy*, Geneva, September 1958, Vol. 6, p. 250.
- SINGH, B. N., EDWARDS, D. J., and TOFT, P., 1996, *J. nucl. Mater.*, **238**, 244; 2000a, Report RISO-R-1213(EN), Risø National Laboratory; 2001, *J. nucl. Mater.* (to be published).
- SINGH, B. N., FOREMAN, A. J. E., and INKAUS, H., 1997, *J. nucl. Mater.*, **249**, 103.
- SINGH, B. N., STUBBINS, J. F., and TOFT P., 2000b, Report RISO-R-1128(EN), Risø National Laboratory.
- SMIDT, F. R., Jr, Report NRL-7078, Naval Research Laboratory.
- SUN, L. Z., GHONIEM, N. M., and WANG, Z. Q., 2001, *Mater. Sci. Engng.* (to be published).
- TRINKAUS, H., SINGH, B. N., and FOREMAN, A. J. E., 1997a, *J. nucl. Mater.*, **249**, 91; 1997b, *ibid.*, **251**, 172.